DOI:
10.1021/acs.molpharmaceut.5b00942

Document Version
Peer reviewed version

Article

Lateral fenestrations in K+-channels explored using MD simulations

Christian Jorgensen, Leonardo Darré, Victoria Oakes, Rubben Torella, David Pryde, and Carmen Domene

Mol. Pharmaceutics, **Just Accepted Manuscript** • DOI: 10.1021/acs.molpharmaceut.5b00942 • Publication Date (Web): 12 May 2016

Lateral fenestrations in K^+-channels explored using MD simulations

Christian Jorgensen,[a] *Leonardo Darré,*[a] *Victoria Oakes,*[a] *Rubben Torella,*[b] *David Pryde*[b] *and Carmen Domene*[a,c*]

[a]Department of Chemistry, King's College London, Britannia House, 7 Trinity Street, London SE1 1DB, UK

[b]Worldwide Medicinal Chemistry, Pfizer Neuroscience and Pain Research Unit, Portway Building, Granta Park, Great Abington, Cambridge CB21 6GS, UK

[c]Chemistry Research Laboratory, Mansfield Road, University of Oxford, Oxford OX1 3TA, UK

[*]Corresponding author: carmen.domene@kcl.ac.uk

Tel: +44 - (0) 2078483868

Keywords: cavities; tunnels; druggability; ion channels

ABSTRACT

Potassium channels are of paramount physiological and pathological importance and therefore, constitute significant drug targets. One of the keys to rationalize the way drugs modulate ion channels is to understand the ability of such small molecules to access their respective binding sites, from which they can exert an activating or inhibitory effect. Many computational studies have probed the energetics of ion permeation, and the mechanisms of voltage gating, but little is known about the role of fenestrations as possible mediators of drug entry in potassium channels. To explore the existence, structure and conformational dynamics of transmembrane fenestrations accessible by drugs in potassium channels, molecular dynamics simulation trajectories were analysed from three potassium channels: the open state voltage-gated channel Kv1.2, the G protein-gated inward rectifying channel GIRK2 (Kir3.2), and the human two-pore domain TWIK-1 (K2P1.1). The main results of this work were the identification of the sequence identity of four main lateral fenestrations of similar length and with bottleneck radius in the range of 0.9 to 2.4 Å for this set of potassium channels. It was found that the fenestrations in Kv1.2 and Kir3.2 remain closed to the passage of molecules larger than water. In contrast, in the TWIK-1 channel, both open and closed fenestrations are sampled throughout the simulation, with bottleneck radius shown to correlate with the random entry of lipid membrane molecules into the aperture of the fenestrations. Druggability scoring function analysis of the fenestration regions suggest that Kv and Kir channels studied are not druggable in practice due to steric constraining of the fenestration bottleneck. A high (>50%) fenestration sequence identity was found in each potassium channel subfamily studied, Kv1, Kir3 and K2P. Finally, the reported fenestration sequence of TWIK-1 compared favourably with another channel K2P channel TREK-2 reported to possess open fenestrations, suggesting that K2P channels could be druggable via fenestrations, for which we reported atomistic detail of the fenestration region, including the flexible residues M260 and L264 that interact with POPC membrane in concerted fashion with the aperture and closure of the fenestrations.

INTRODUCTION

The term 'druggability' refers to the ability of a small molecule to modulate the function of a target receptor protein. It is estimated that 10-15% of the genes identified by the Human Genome Sequencing Consortium constitute useful druggable targets, of which only half may constitute real protein targets.[1] Due to their vast range of physiological roles, ion channels are of paramount pharmacological importance, and are targets for over 20% of drugs on the market.[2] Potassium channel druggability mechanisms remains an active area of research, for which no single unified mechanism is known.[3] Potassium channels form selective pores that span cell membranes, enabling the selective and rapid conduction of potassium ions down the electrochemical gradient.[4] Their structure comprises two or four subunits, forming dimers of dimers or tetramers. A pore-loop structure lines the top of the pore, known as the selectivity filter that modulates the selective ion permeability. Currently, at least 60 unique potassium channel X-ray crystal structures are available,[3] of which representatives of three families of potassium channels were considered here.

The first channel employed in this study belongs to the voltage-gated (Kv) channel family which spans at least nine known subfamilies, Kv1-9.[5] Small-molecule druggability of the Kv1 subfamily has been proposed to occur via a cooperative mechanism involving two main blocking sites: the inner-pore site, located below the selectivity filter, and a side-pocket cavity located between the pore and the voltage-sensor, for which it is thought fenestrations could play an active role in modulating the blockage mechanism.[6-8] Current well-established inner-pore Kv1 blockers include 4-aminopyridine (4-AP), tetraethylammonium (TEA),[9] tetrabutylammonium (TBA),[10] and correolide.[11] Due to the highly conserved inner-pore sequence, these drugs do not show specificity among Kv1 subtypes, which has hindered further therapeutic applications. A new generation of phenoxyalkoxypsoralen derivatives has shown increased Kv1 subtype specificity, and holds therapeutic promise.[12-13] Kv1.2 is an active druggable target for neurological and autoimmune disorders such as multiple sclerosis, type-1 diabetes mellitus and rheumatoid arthritis.[12-13]

The second channel employed belongs to the inward-rectifying (Kir) channels, which preferentially conduct current in the inward direction into the cell. Kir channels constitute therapeutic target for many common disorders including hypertension, cardiac arrhythmia and pain.[14] Kir channels span at least seven subfamilies, Kir1-7, with the Kir3 subfamily having their activity critically regulated by G protein-coupled receptors (GPCRs).[15] Thus they are referred to as GPCR-activated Kir (GIRK) channels. The broad range of Kir-

regulatory functions means that some Kir channels occupy a unique physiological 'niche'.[15] Kir3.2 small-molecule druggability is currently limited to nonselective cardiovascular and neurological drugs with off-target activity toward Kir channels. This means that the real therapeutic potential and druggability of most Kir channels has not yet been determined experimentally.[15] Current work on neuronal Kir3 (GIRK) pharmacology has focused on well-studied neurological drugs, all of which exhibit low affinity toward GIRK, including the serotonin-reuptake inhibitor fluoxetine,[15-16] as well as pore-blocking opiates, small-molecule analgesics for pain management. Crucially, a clear understanding of the potential of neutral GIRK channels in pain requires the development of selective Kir3.1/Kir3.2 small-molecule drugs.[15] A mechanistic understanding of drug binding pathways and knowledge of specific chemical sequence of fenestrations may prove useful for this purpose. An example of a common small-molecule pore blocker, Vernakalant, reached clinical trials and showed efficacy in terminating the onset of atrial fibrillation. However, Vernakalant also inhibits the cardiac Kv1.5 and Kv4 channels by blocking the highly conserved Kv family pore, thus precluding further therapeutic assays.[17]

The third and final channel studied belongs to the two pore domain potassium (K2P) channels, which generate leak potassium currents, and thus plays an essential role in cell excitability. K2P channels have been proposed to show weak inward rectification,[18-19] suggesting resemblance with/to inward-rectifying (Kir) potassium channels.[19] Six subfamilies, TWIK, TREK, TALK, TASK, THIK, and TRESK have been identified, primarily implicated in a range of cardiovascular and neurological disorders. A unique structural attribute of K2P channels is the absence of the classical cytoplasmic bundle crossing rendering structural changes at the selectivity filter, the primary mode of gating.[20-22] The crystal structure of TWIK-1 helped elucidating the topology of the plasmatic membrane. A vast range of regulatory stimuli are proposed to modulate this gate,[23] such as hydrophobic compounds and various lipids that readily enter the membrane bilayer through lateral fenestrations.[24] Small molecule block of K2P channels is currently limited to the targeting of TREK-1. K2P channels are poorly inhibited by classical K^+ channel blockers such as TEA, Cs^+ and 4-aminopyridine when applied from the extracellular site, but it has recently been shown that a known family of Kv1 blockers, the quaternary ammonium (QA) ions, potently block TREK-1 when applied from the intracellular side.[25] In Kv and Kir channels, QA ions are known to bind from the intracellular side by binding to a site deep within the pore just below the selectivity filter (the pore site). K2P block has been studied with spadin, a sortillin-

derived peptide, which has been identified as a novel antidepressant treatment,[26] but with no reported binding site. Sortillin binding has been reported to be akin to fluoxetine inhibition of TREK-1, which does not target the pore, but instead a C-terminal site.[27] In addition, a series of substituted caffeate esters have been shown to relieve pain by targeting TREK-1, and therefore might contribute to the next generation of analgesic drugs.[28]

To understand the mechanism of drug modulation of ion channels, it is necessary to understand the location of small molecule binding sites, and how they can be accessed. Drug binding depends both on the target conformational state (open, closed or inactivated), as well as the real-time dynamics of the residues lining the fenestrations and entry tunnels of the target. Many studies have probed the energetics of potassium ion permeation,[29-32] and the mechanisms of gating,[33-35] but little is known about the role and presence of fenestrations in potassium channels. Work on fenestrations in Kir1.1 channels found a specific cholesterol binding pocket accessible from the membrane via lateral fenestrations by docking studies.[36] Such a cavity was proposed to be absent in Kir2.2 and Kir3 from sequence alignment. Additionally, bound molecules were identified in the fenestration regions of the X-ray crystal structures of the TWIK-1[20] and TREK-2 (K2P10.1)[37], specifically lipid density in TWIK-1 fenestrations, and norfluoxetine (the active metabolite of Prozac) bound to TREK-2 fenestrations. Comparison of TREK-2 structures in multiple activation states revealed distinct structural differences in the spatial attributes of fenestration regions, implicating 'open' fenestrations, and key residues within them, in the state-dependent block of TREK-2 by Prozac.

In this work, we are utilizing the predictive power of computational modelling to characterize the fenestration regions in other potassium channels where crystal structures in several activation states are unknown, or the presence of fenestrations has not been examined in detail, in order to assess the accessibility, and hence potential druggability of such regions. The availability, topology and conformational dynamics of lateral fenestrations in the transmembrane domain of three potassium channels are studied using MD simulation trajectories comprising around one microsecond of accumulated sampling. The channels selected are, the voltage-gated potassium ion channel Kv1.2, the inward-rectifying GPCR-activated Kir3.2 (GIRK2) channel, and the two-pore domain channel TWIK-1 (K2P1.1). The results are compared to the reported X-ray structure of TREK-2 in complex with norfluoxetine.[37] The information reported may potentially aid in the design of next generation potassium channel blocking drugs.

METHODS

Systems Set-up

Molecular Dynamics (MD) simulations were carried out on the structure of open-state Kv1.2 (PDB id 3LUT, resolution 2.9 Å),[38] the close -and open states of the murine G protein-gated inward rectifying K^+ channel GIRK2 (Kir3.2) (Kir3.2/C: PDB id 3SYA, resolution 2.98 Å,[39] and Kir3.2/O: PDB id 3SYQ, resolution of 3.44 Å,[39] respectively) and of the open-state human two-pore domain potassium channel TWIK-1 (PDB id 3UKM, resolution 3.4 Å)[20] (Figure 1). The initial structure of missing the loops in Kir3.2/O (residues 70-80 or 67-81 in chains A or B respectively, and 118-133 in both chains) was generated using MODELLER 9.11,[40] and the crystal structure of the murine Kir3.2 solved in complex with the beta-gamma G protein subunits (PDB id: 4KFM) as template,[41] as it contains the required loops. For TWIK1-1, residues 18-281 were used to for the structure of TWIK-1, and missing residues residues (95-99 and 169-174) were modelled using Modloop[42] in MODELLER.

The pore of each channel was initially hydrated by employing the SOLVATE software,[43] which facilitates the hydration of irregularly shaped solutes, particularly relevant in filling the central pore of the channels. The resulted system was then embedded in a pre-equilibrated lipid bilayer of 1-Palmitoy-l,2-oleoyl-sn-Glycero-3-phosphocholine (POPC) molecules, with the central pore axis aligned to the bilayer normal. Lipid molecules overlapping with protein atoms were removed. A rectangular box of dimensions specific to each system was used to centre the system, and the void space was filled with water molecules using the Solvate plugin of VMD, removing those overlapping with protein or lipid atoms. Potassium and chloride ions were added to the system to achieve neutralization up to a final concentration of 150 mM to mimic a biological environment. Three potassium ions in the selectivity filter of the crystal structures were kept. In addition, in the case of Kir3.2/C, four sodium ions (one per subunit) present in the crystal structure were also included. PIO ([(2R)-2- octanoyloxy-3-[oxidanyl-[(1R,2R,3S,4R,5R,6S)-2,3,6-tris(oxidanyl)-4,5-diphosphonooxy- cyclohexyl]oxy-phosphoryl]oxy-propyl] octanoate) molecules present in both crystal structures of Kir3.2 were used to reconstruct the PIP2 molecules proposed to bind in each state of the channel. The same stoichiometry as observed in the crystal structures was kept in the simulated systems, i.e. four and two PIP2 molecules for the close and open states, respectively. Recently developed CHARMM parameters for PIP2 were used.[44] The CHARMM 36 force field[45] was used for the lipids, CHARMM 27[46] was used for the protein, the TIP3P model[47] was used for water, and the standard CHARMM parameters and NBFIXES were used for the

ions.[48]

Molecular Dynamics simulations

The NAMD2.9[49] software was used to perform the computations. Each system was subjected to 5,000 steps of energy minimization followed by a set of MD equilibration steps in the NpT ensemble including, using a 1 kcal/mol/Å^2 force constant throughout: (i) 500 ps applying restraints on the protein, the water in the pore cavity, and the crystallographic potassium ions fixed to the crystal structure. The NAMD Tcl Forces module was used to avoid hydrating the void space in the hydrophobic interface between the channel transmembrane domain and the membrane by applying an inverse force on water molecules crossing the hydrophobic interface, thereby excluding them, while the lipids pack around the protein; (ii) 500 ps applying restraints on the protein backbone atoms, relaxing the solvent in the cavity and the amino-acid side chains; (iii) 500 ps applying restraints on the protein atoms; (iv) 500 ps applying restraints on the selectivity filter alone. Semi-isotropic pressure coupling at 1 atm was accomplished using the Nose-Hoover Langevin piston using a damping time constant of 50 fs and a period of 200 fs, while temperature was maintained at 310 K by means of the Langevin thermostat with a damping coefficient of 1 ps^{-1}. Long-range electrostatic interactions were treated using the particle mesh Ewald algorithm with a grid spacing of 1Å and van der Waals forces were smoothly switched off between 10-12 Å, NAMD defaults for spline and κ values.[50] A Verlet neighbour list with pairlist distance of 13 Å was used. The lengths of covalent bonds involving hydrogen atoms were constrained by the SETTLE algorithm in order to use a 2-fs time-step. The multi time step algorithm Verlet-I/r-RESPA was used to integrate the equations of motion. Non-bonded short-range forces were computed every time step, while long-range electrostatic forces were updated every two time steps. The total available MD production runs amount to 0.8 μs. The Kir3.2/O trajectory was of 100 ns, the TWIK-1 trajectory of 200 ns, and the Kv1.2 trajectory of 400 ns. An additional 100 ns trajectory of Kir3.2 closed state (Kir3.2/C) was used to compare the Kir3.2/O result.

Fenestration search

The output of the MD simulation trajectories of each channel were scanned for fenestrations using the CAVER 3.0 software,[51] in which the outer surface of the protein is calculated by rolling a large spherical probe around its surface, and then internal fenestrations are identified using a probe comprising 12 spheres of radius 0.8 Å. All identified fenestrations are then

grouped into clusters based on relative proximities and with an 8 Å cut-off for each cluster node. In this way, fenestrations differing from the node by more than 8 Å are excluded.

Residues lining the fenestrations were compared using a multiple sequence alignment considering Kv1.2 (Uniprot P16389), Kv1.3 (Uniprot P22001), Kv1.5 (Uniprot P22460), Kv7.1 (Uniprot P51787), mammalian Kir3.2 (Uniprot P48542), Kir3.1 (Uniprot P48549), Kir2.2 (Uniprot Q14500), human TWIK-1 (TWIK-1; Uniprot O00180), K2P10 (TREK-2; Uniprot P57789) and K2P6.1 (TWIK-2; Uniprot Q9Y257) employing the ClustalO[52] algorithm. Electrostatic potential iso-surface calculations were performed using APBS v1.4,[53] with results presented in the Supplementary Material, Figures S3 and S4.

Pfido druggability scoring function analysis

The cavity analysis is a useful tool for obtaining specific residues and physical parameters about the dimensions of fenestrations, however, it does not provide a quantitative indication of the likelihood or druggability of fenestration sites, as quantified by e.g., the binding free-energy at the site. Pfido[54] is a relevant alternative method, which can yield a druggability score (kcal/mol) for each channel. Pfido is a druggability prediction method developed by Pfizer that aims to predict the druggability of pharmaceutical targets based solely on the binding-site structure. A Pfido calculation requires the definition of a binding site and a ligand probe. Norfluoxetine was chosen as the probe for these systems. The binding site was represented using computational geometry methods,[55-56] and defined as the cavity spanned by fenestrations residues in a 5Å radial distance from the molecule probe origin. Three parameters were used to quantify the druggability of the binding: fraction lipophilic (non-polar) surface area (SA), fenestration surface curvature and calculated druggability score. The calculated druggability score (kcal/mol) is the maximal affinity predicted (MAP) binding energy ΔG_{MAP}, equation (1), which is an estimate of the maximal achievable affinity for a binding pocket from a hit-to-lead optimization effort.

$$\Delta G_{MAP} \simeq -\gamma(r) SA_{np}^{target} \left(\frac{SA_{druglike}^{target}}{SA_{total}^{target}} \right) + C \qquad \text{Equation (1)}$$

Here, $\gamma(r)$ describes the solvent surface tension, and depends on the surface curvature. The curvature was estimated from a least squares fit (LSF) of a sphere to a surface patch. The total surface area of the pocket, SA_{total}^{target} is a normalization factor to the drug-like surface area $SA_{druglike}^{target}$ size set to 300 $Å^2$ (Table 2). The constant C accounts for the ligand desolvation free-energy and assumes that the lipophilic surface area is constant. The fraction lipophilic surface

area is a direct measure of the ratio between the lipophilic surface area and the polar surface area (SA_{np}^{target}) of the binding site, while the curvature gives a three-dimensional representation of the binding-site shape. The output druggability score ΔG_{MAP} (kcal/mol) was converted to a nM affinity K_d value through equation (2) where R is the gas constant in units kcal/mol/K, and T is 298 K.

$$K_d=\exp(\Delta G_{MAP}/RT) \qquad \text{Equation (2)}$$

The Pfido analysis was obtained for each potassium channel using five representative structures from the MD simulations chosen at intervals of 10 ns from the last 50 ns of simulation for each potassium channels, with the error estimates reported as one standard deviation ($\pm\sigma$).

RESULTS AND DISCUSSION

To establish the stability of the proteins during the simulation, changes in the backbone root-mean-square deviation (RMSD) of each structure with respect to the crystal with time were calculated and shown in Figure S1. In all cases, the RMSD remains stable (<2 Å). In all three systems simulated, four clusters of lateral fenestrations were found and are illustrated in Figure 1.a,c and 2.a,b,c, with over 70% of analysed snapshots having fenestrations with bottleneck radius greater than the threshold 0.8 Å (Table 1). For each system the analysis was repeated at subsets of the whole trajectory length to show reproduction of the results obtained here were consistent over the timescales analysed. For Kv1.2, fenestration analysis was repeated for the first 100, 200 and 400 ns of simulation, yielding fenestration parameters within same standard deviation of statistical error (Supp. Mat. Table S3). For K2P, the available 200 ns trajectory was analysed for the first 100 and 200 ns, obtaining the same results (Supp. Mat. Table S4).

In Kv1.2 the lateral fenestrations are formed at the interface of adjacent subunits, and can therefore be referred to as inter-chain tunnels. TWIK-1 is a structural homo-dimer, possessing a pseudo-tetrameric architecture, with two tunnels on the dimer interface (lateral-A/B) and an additional set at the interface between individual domains (intra-subunit) within each subunit (lateral A and lateral B), in analogous positions to those in Kv1.2, yet displaying asymmetry between each subset. In Kir3.2, the lateral fenestrations correspond to pathways across individual subunits, also denoted intra-chain tunnels. Inter-chain fenestrations, similar to Kv1.2 and TWIK-1, are also found in Kir3.2, but with low populations (<40 %),

suggesting that they are less favourable in Kir3.2. Such lateral fenestrations are similar to what it is observed for Nav channels.[57] Results indicate that, within each analysed channel, no significant differences between lateral fenestration lengths exist (Table 1).

Fenestrations can be classified in two functional states depending on their bottleneck radius (BR): open and closed. In this work, an arbitrary cutoff of 1.6 Å was employed to discriminate between closed (BR<1.6 Å) and open (BR>1.6 Å) fenestrations. In all three systems simulated, the identified fenestrations proved stable with time. In the case of the simulations of Kv1.2 and Kir3.2, closed fenestration states with an average bottleneck radius of ~1 Å are sampled, with maximum values up to 1.6 Å (Figure 3.d,f). In the closed fenestration state, only transient (~1-2 ns) pore access is available for water-sized molecules.

In the TWIK-1 X-ray crystal structure, the inter-chain fenestrations show bottleneck radii of 2.5 Å. Upon simulation with this density removed, the fenestrations display average BR of 1.4 ± 0.5 Å and 1.0 ± 0.2 respectively (Figure 2.i). The former fenestration is able to sample the open fenestration state (maximum opening of 2.5 Å), with the latter consistently in the closed state (BR of ~1 Å) resembling that in Kv1.2 and Kir3.2 (Figure 2.h,i). The values indicate that TWIK-1 fenestrations are mainly closed, as in Kv1.2 and Kir3.2, but they can spontaneously sample open states by adopting a BR close to that in the TWIK-1 X-ray structure.

To study the characteristics of the bottlenecks in detail, the fenestration radius along the progression from the outside of the membrane to the inside toward the central pore was measured, and it is shown in Figure 4 for each analysed fenestration of Kv1.2, Kir3.2 and TWIK-1. One main constriction site is observed in all four lateral fenestrations. The reduction of the radius at that position is due to the presence of residues V399, I402 and A403 in Kv1.2, T105, E152, G180 and V183 in Kir3.2, and V139, I142, P143, F220, S224, M260, L264 in TWIK-1 (Supplementary Table S2 and Figure 4).

The amino acid composition and sequence alignment of the main fenestration lining residues for Kv1.2, Kir3.2 and TWIK-1 is reported in Supplementary Table S2, the consensus set of contacts is illustrated in Figure 3.b,c,d, and the bottleneck-lining residues are illustrated in Figure 4.a,b,c. For Kv1.2, the lining residues are L328, I332, A397, V399, L400, T401, I402, A403, V406, P407, and V410 in each monomer (Figure 3.b). This path appears to be flanked with a higher content of hydrophobic (82%) than polar residues (18%). For Kir3.2 the main lining residues in each lateral fenestration are V188, N184, V183, G180, L179, T154, T153,

E152, W106, T105, V104, Y102 and V101 (Figure 3.c). The path in Kir3.2 appears more hydrophilic with 46% of hydrophobic residues, 46% of polar residues and 8% of negatively charged residues. For TWIK-1, the main lining residues for intra-subunit fenestrations (fenestrations 1 and 2) are S116, T117, T145, L146, L149, T225, L254 and L257, constituting 50% polar residues, while for inter-chain fenestrations (fenestrations 3 and 4) T117, V139, I142, L146, S224, T225, M260, L261 and L264, constituting 45% polar residues (Figure 3.d), with the remaining residues of both sets hydrophobic. The residues responsible for the equilibrium between open and closed fenestration states in TWIK-1 were identified as M260 and L264 (Figure 5.a,b,c,d), with a transition time on the order or 10^1 ns (Figure 5.f), meaning that MD simulations can adequately capture this side-chain movement on a 200 ns simulation scale. Fenestration accessibility for lipids was considered by occupancy density iso-surfaces (Figure S5), which reveal lipid density only around Kv1.2 and Kir3.2 fenestrations on the iso-0.2 surface, without any lipid entry observed. For TWIK-1, lipid penetration at the periphery of the inter-subunit (A/B) fenestrations (3,4) was observed (Figure 5.a,b). The lipid entry correlates with a bottleneck radius > 1.5 Å (Figure 5.e compared to Figure 5.f).

It was considered if a correlation exists between the channel activation state and fenestration opening. The open, activated Kv1.2 channel has only closed fenestrations, while the open, activated Kir3.2 channel state and the closed Kir3.2 channel states both possessed closed fenestrations. For TWIK-1, lipid penetration at the periphery of the inter-subunit (A/B) fenestrations (3,4) was observed (Figure 5.a,b), and the lipid entry correlates with a bottleneck radius > 1.5 Å (Figure 5.e compared to Figure 5.f). The bottleneck radius fluctuation correlates with the M260-L264 distance and the fenestration-lipid distance, as was shown in Figure 5.e compared to Figure 5.f. Channel conformational changes, in particular those responsible for the opening or closing processes, can affect the structure of the lateral fenestration and consequently, drug accessibility. This has been reported to depend on the channel type. In TREK-2, changes in functional state impacts the availability of the fenestrations.[37] Comparison of TREK-2 structures in multiple activation states revealed distinct structural differences in the spatial attributes of fenestration regions, implicating ‘open’ fenestrations, and key residues within them, in the state-dependent block of TREK-2 by Prozac. Analysis of the fenestrations from MD simulations in both the open and closed states of Kir3.2 (Table 1) showed that both states possessed the four reported fenestrations with similar average and maximum bottleneck radii, as well as similar fenestration length,

suggesting that fenestrations are not state-dependent in this case.

To supplement these results, a Pfido druggability analysis was performed on MD snapshots of the fenestration regions of Kv1.2, Kir3.2, TWIK-1 (Table 2), and compared to the crystal structure of TREK-2.This analysis revealed Kir3.2 fenestrations to be outliers, possessing half the magnitude of hydrophobic surface-area (165 ± 21 $Å^2$) compared to the other channels (Kv1.2: 399 ± 28 $Å^2$; TWIK-1: 387 ± 25 $Å^2$; TREK-2: 401 $Å^2$), with double the magnitude of polar surface area (122 ±15 $Å^2$) compared to the other channels (Kv1.2: 42 ± 6 $Å^2$; TWIK-1: 30 ± 5 $Å^2$; TREK-2: 85 $Å^2$). This surface-area analysis was then complemented by an electrostatic potential (EP) iso-surface analysis of Kv1.2, Kir3.2 and TWIK-1 (Figure S3 and S4). The analysis revealed that Kv1.2 fenestrations containing 82% hydrophobic residues displayed their EP iso-surface uniformly around zero, while the Kir3.2 iso-surface showed the presence of polar lining residues in the fenestrations (N184 and Y102 in each fenestration). The Pfido analysis outputs a druggability score of magnitude < -10 kcal/mol for all channel fenestrations studied herein, with more negative score indicating greater druggable potential. By calculating K_d values and comparing to reference datasets of targets,[54] it is possible to class the channels as potentially druggable, because with their nM affinity druggability scores K_d (Table 2) all range between 10^{-3} to 38 nM, which according to data set comparisons ranks as druggable targets with K_d<100 nM.[54]

To understand the role of chemical sequence in fenestrations, a multiple sequence alignment was generated for mammalian Kv1.2, Kv1.3, Kv1.5, Kv7.1, Kir3.2, Kir3.1, Kir2.2, human TWIK-1, TREK-2 and TWIK-2(Figure 3.a). This reveals that the lining residues of the fenestrations in Kv1.2, Kir3.2 and TWIK-1 share a common region in the sequence, where residues T154 and T153 in Kir3.2 correspond to S224 and T225 in TWIK-1, or T280 and T281 in TREK-2; L179 in Kir3.2 is conserved as L400 in Kv1.2; G180 in Kir3.2 corresponds to T401 in Kv1.2; V183 in Kir3.2 is conserved as V262 in TWIK-1, while the latter is not a lining residue. Finally, N184 in Kir3.2 was not conserved, and corresponded to V263 in TWIK-1 and P405 in Kv1.2. In addition, the TWIK-1 fenestration bottleneck shares a common region with the sequence of TREK-2 (K2P10.1). The TREK-2 fenestration residues when binding norfluoxetine were reported to be I194, P198, C249, V253, V276, L279, T280, F316 and L320.[37] Crucially, fenestration residues M260 and L264 in TWIK-1 correspond to fenestration residues F316 and L320 in TREK-2 as shown in Figure 3. This high similarity in fenestration bottleneck sequence could suggest that drugs targeting TREK-2 could also target TWIK-1, and that agonist/antagonist mechanisms of K2P channels could be similar.

Previous MD simulation studies reported the sequence conservation of fenestration-lining residues in sodium channels to be generally high,[57] and claimed this to be higher than the reported low conservation in other ion channel families, including potassium channels, but did not distinguish between sequence identities among different sodium subfamilies. In this work, potassium channel sequence alignment found low global sequence conservation, with only ~4% of the transmembrane domains of mammalian Kv1.2, Kir3.2 and TWIK-1 conserved, and a ~2% of local transmembrane fenestration sequence identity. However, potassium channel subfamilies display very high fenestration identities, 86% for Kv1 subtype members, 63% for Kir3 subfamily members, and 47% for the K2P1 subfamily members. While previous studies have claimed to find higher conservation in sodium channels, these they reported only Nav channel subfamily identities to be above 50%,[57] which is not different from our reported sequence conservations. These higher identities thus suggest a common role for fenestrations in individual potassium channel subfamilies may be possible. This work has complemented earlier work on TREK-2,[37] by identifying open fenestrations in a second K2P channel, TWIK-1, and has concluded that the size of fenestrations renders this unlikely in Kv1.2 and Kir3.2 In this case, if the role of fenestrations in drug access is of secondary importance, it has been proposed that fenestrations bestow conformational flexibility on the pore domain, and thus play a role in gating.[58] Previous studies on fenestrations in voltage-gated sodium ion channels reported well-conserved fenestration-lining residues.[59]

Links between fenestrations and druggability

The blocking mechanism in Kv1.2 and Kv1.5 channels have been described as involving two primary binding sites: an inner pore site with sequence T…VIAV, and a non-pore site with sequence LLL...FIL...T,[6, 8] with locations conserved across Kv1 and non-Kv1 members. In Kv1.2, the non-pore site is located in a voluminous side-pocket cavity delineated by residues L317 and L321 from the S4-S5 linker, F334, I337, and L341 from the S5 helix, and T401 from S6 helix.[8] In Kv1.5, the non-pore site is located in a cleft delineated by contacts L420, L423, L427, F440, I443, L447, and T507.[6] In open-state Kv7.1, the non-pore site is located in a side-pocket of contacts L250, L251, and V254 in the S4-S5 linker, together with the phenyl ring of F351 from the S6 helix.[60] The pore site alone is most likely unable to confer the acute selectivity of a given drug for different Kv channels, mainly because the sequence of the inner pore is conserved among Kv channels, as well as due to the vast chemical range of Kv inner-pore blockers, namely 4-AP, TEA,[9] TBA,[10] and correolide.[11] It has been argued that selectivity for a given drug arises from a putatively allosteric or cooperative interplay

between the pore site and a side-pocket in Kv1.2,[8] and Kv1.5.[6] Psora-4 and PAP-1 of the 5-phenylalkoxypsoralen family of drugs, designed to target autoimmune disorders[12-13] were found to show Kv1 subtype specificity by cooperatively interacting with both the inner pore and the non-pore site.[6, 8] The fenestration lining residues identified herein for Kv1.2 is partially in agreement with the residues constituting the Kv1 side-pocket, suggesting that the potential for cooperative interactions is a possibility. As suggested for the blocking mechanism in Kv1.3 and Kv1.5 (Psora-4 block),[6, 13] and Kv2.1 (Flecainide and Propafenone block), the existence of lateral fenestrations connecting the pore and side-pocket sites might allow for allosteric interactions were the bottleneck radius larger.[6, 8] The bottleneck radius sampled in the MD simulations revealed it to be too small to allow the aromatic ring of PAP-1 to percolate from the side pocket to the inner pore. This suggests that the cooperative effect between the side-pocket and the inner pore pocket in Kv1.2 is more probable to be mediated by the protein residues lining the fenestrations than a result of direct contacts between drugs located in such pockets. Alternatively, conformational changes taking place in a time-scale not accessed by the MD simulations presented here could be responsible for widening the bottleneck of the lateral fenestrations. Similarly, for the Kir3.2 channel in both open and close conformations, the bottleneck radius sampled during the simulations corresponds only to closed fenestration states. On average, the size of the fenestration is too small to allow the entrance of even water molecules, except for very short time periods (1-2 ns) where maximum bottleneck radius of ~1.5 Å are observed.

For TWIK-1 the inter-subunit fenestrations can sample an open fenestration state during the MD trajectory (Table 1), and additionally, the X-ray crystal structure of the ‘open state’ TWIK-1 is argued here to compare to the ‘down state’ of TREK-2,[37] (Supporting Table S1 and Figure 1.c,d) owing to its helical arrangement and the presence of such open inter-subunit fenestrations. Both structures contained lipid density in the fenestrations, with TREK-2 having the bound drug norfluoxetine in the fenestrations. However, TREK-2 fenestrations are only observed in the ‘down state’ (the putative closed or inactivated channel state).[37] In the absence of norfluoxetine, the up-state conformation is adopted, and two hydrophobic residues, F316 and L320, occlude the fenestration as a consequence of the conformational transition. Thus, fenestration dynamics explains the state selective binding and action of norfluoxetine in TREK-2. In line with these observations, inter-subunit fenestrations in TWIK-1 predominantly adopt a closed conformation throughout the simulations, likely due to the removal of crystallised lipids during simulation setup. However, an inter-conversion

between closed (BR ~ 1.0 Å) and open (BR > 2.0 Å) fenestration states occurs throughout, providing ample opportunities for the entrance of lipid molecules and small drug compounds. This process appears to correlate with the extent of constriction between M260 and L264 residues (Figure 5.c,d). The position of these residues is conserved with respect to TREK-2 (F316 and L320), suggesting potential implications across the K2P family.

The result found on the open state of TWIK-1 suggests that it behaves qualitatively like the up-state of TREK-2 with closed fenestration states, but that it is able to also sample the open fenestration states reported in the 'down-state' of TREK-2.[37] Our results support the existence of a wide enough hydrophobic fenestration bottleneck in TWIK-1, which is mostly closed but can spontaneously open to allow for hydrophobic compounds to enter and either bind or access the pore via the lateral fenestrations.[24] This could contribute to the understanding of how the TWIK-1 pore gate is modulated by a large range of regulatory stimuli and molecules, as suggested experimentally.[23]

CONCLUSIONS

In this study, MD simulation trajectories of three representative potassium channels have been used to investigate the presence and chemical characteristics and structural dynamics of lateral fenestrations, for which four fenestrations are identified in each channel. Additionally, over the time course of the simulations, no statistically significant fluctuations in fenestration length were recorded suggesting that transient fast protein side-chain motions and rotations do not appear to exert significant effects upon fenestration lengths. From bottleneck radius analyses, results indicate that the fenestrations in Kv1.2 and Kir3.2 could not modulate drug access (BR ~1.0 Å), while in the case of TWIK-1 (maximum BR of 2.5 Å), the fenestrations can potentially work as drug access pathways. It was shown that the rise in bottleneck radius correlates with the entry of lipid molecules into TWIK-1 fenestrations, which is then argued to be responsible for allowing TWIK-1 to sample both open and closed fenestrations. While our analysis shows Kv1.2 and Kir3.2 fenestrations to be closed, experiments have found Kv channel fenestrations to have the possibility of undergoing conformational rearrangements of lining residues to turn on the ability of binding drugs, with a recent X-ray crystal of KcsA containing the known Kv blocker QA ion bound in the fenestration region in the inter-subunit space, akin to the fenestrations 1-4 of Kv1.2 reported here, thus, the potential for druggable Kv1 and Kir3 targets can not be ruled out.[61] The existence of slow transitions at timescales above 100 ns, which cannot be sampled with ns MD timescales suggests that the next step in fully mapping the significance of the Kv1 and Kir3 fenestration regions in perturbing protein

structure and function,

TWIK-1 exhibited asymmetry in its fenestrations, with the side-chains of M260 and L264 responsible for the channel sampling an equilibrium state between closed and open fenestration, with state lifetimes on the order of 10^1-10^2 ns. In the open state of TWIK-1, the fenestrations are mainly closed, but can also sample the open fenestration state. Because the reported fenestration sequence of TWIK-1 had overlap with that of TREK-2, including the identification of bottleneck residues M260 and L264 that are in correspondence with TREK-2 fenestration residues F316 and L320, with the latter channel reported to possess open fenestrations, it is concluded that K2P channels could be druggable via fenestrations. We reported atomistic detail of the fenestration region, including the flexible residues M260 and L264 that interact with POPC membrane in concerted fashion with the aperture and closure of the fenestrations.

In conclusion, the study identified four lateral fenestrations across the range of potassium channels studied. Using structural and sequence alignment, a detailed analysis was given of how these identified fenestrations differ among the K^+-channel subtypes analysed. This information provides a framework for rationalizing the differential response of potassium channels to drugs targeting the transmembrane domain.

ACKNOWLEDGMENTS. We would like to acknowledge the use of computational resources from the EPSRC UK National Service for Computational Chemistry Software (NSCCS), the Hartree Center, and Archer. This work was supported by the Engineer and Physical Sciences Research Council (EPSRC) and the Biotechnology and Biological Sciences Research Council (BBSRC). C. Jorgensen thanks King's College London for a Graduate Teaching Assistance studentship. V. Oakes is supported by a CASE studentship funded by BBSRC and Pfizer Neusentis.

REFERENCES

1. Grigoriadis, D. E.; Hoare, S. R. J.; Lechner, S. M.; Slee, D. H.; Williams, J. A., Drugability of Extracellular Targets: Discovery of Small Molecule Drugs Targeting Allosteric, Functional, and Subunit-Selective Sites on GPCRs and Ion Channels. *Neuropsychopharmacology* **2008,** *34* (1), 106-125.
2. Huang, X.; He, Y.; Dubuc, A. M.; Hashizume, R.; Zhang, W.; Reimand, J.; Yang, H.; Wang, T. A.; Stehbens, S. J.; Younger, S.; Barshow, S.; Zhu, S.; Cooper, M. K.; Peacock, J.; Ramaswamy, V.; Garzia, L.; Wu, X.; Remke, M.; Forester, C. M.; Kim, C. C.; Weiss, W. A.; James, C. D.; Shuman, M. A.; Bader, G. D.; Mueller, S.; Taylor, M. D.; Jan, Y. N.; Jan, L. Y., EAG2 potassium channel with evolutionarily conserved function as a brain tumor target. *Nature Neuroscience* **2015,** *18* (9), 1236-1246.
3. Fernández-Ballester, G.; Fernández-Carvajal, A.; González-Ros, J. M.; Ferrer-Montiel, A., Ionic Channels as Targets for Drug Design: A Review on Computational Methods. *Pharmaceutics* **2011,** *3* (4), 932-953.
4. Choe, S., Ion Channel Structurepotassium Channel Structures. *Nature Reviews Neuroscience* **2002,** *3* (2), 115-121.
5. MacKinnon, R., Potassium channels. *FEBS Letters* **2003,** *555* (1), 62-65.
6. Marzian, S.; Stansfeld, P. J.; Rapedius, M.; Rinné, S.; Nematian-Ardestani, E.; Abbruzzese, J. L.; Steinmeyer, K.; Sansom, M. S. P.; Sanguinetti, M. C.; Baukrowitz, T.; Decher, N., Side pockets provide the basis for a new mechanism of Kv channel–specific inhibition. *Nature Chemical Biology* **2013,** *9* (8), 507-513.
7. Seebohm, G., Molecular Determinants of KCNQ1 Channel Block by a Benzodiazepine. *Molecular Pharmacology* **2003,** *64* (1), 70-77.
8. Jorgensen, C.; Darré, L.; Vanommeslaeghe, K.; Omoto, K.; Pryde, D.; Domene, C., In Silico Identification of PAP-1 Binding Sites in the Kv1. 2 Potassium Channel. *Molecular pharmaceutics* **2015,** *12* (4), 1299-1307.
9. Grissmer, S.; Nguyen, A. N.; Aiyar, J.; Hanson, D. C.; Mather, R. J.; Gutman, G. A.; Karmilowicz, M. J.; Auperin, D. D.; Chandy, K. G., Pharmacological characterization of five cloned voltage-gated K+ channels, types Kv1. 1, 1.2, 1.3, 1.5, and 3.1, stably expressed in mammalian cell lines. *Molecular Pharmacology* **1994,** *45* (6), 1227-1234.
10. Zhou, M.; Morais-Cabral, J. H.; Mann, S.; MacKinnon, R., Potassium channel receptor site for the inactivation gate and quaternary amine inhibitors. *Nature* **2001,** *411* (6838), 657-661.
11. Koo, G. C.; Blake, J. T.; Shah, K.; Staruch, M. J.; Dumont, F.; Wunderler, D.; Sanchez, M.; McManus, O. B.; Sirotina-Meisher, A.; Fischer, P.; Boltz, R. C.; Goetz, M. A.; Baker, R.; Bao, J.; Kayser, F.; Rupprecht, K. M.; Parsons, W. H.; Tong, X.-C.; Ita, I. E.; Pivnichny, J.; Vincent, S.; Cunningham, P.; Hora, D.; Feeney, W.; Kaczorowski, G.; Springer, M. S., Correolide and Derivatives Are Novel Immunosuppressants Blocking the Lymphocyte Kv1.3 Potassium Channels. *Cellular Immunology* **1999,** *197* (2), 99-107.
12. Schmitz, A., Design of PAP-1, a Selective Small Molecule Kv1.3 Blocker, for the Suppression of Effector Memory T Cells in Autoimmune Diseases. *Molecular Pharmacology* **2005,** *68* (5), 1254-1270.
13. Vennekamp, J., Kv1.3-Blocking 5-Phenylalkoxypsoralens: A New Class of Immunomodulators. *Molecular Pharmacology* **2004,** *65* (6), 1364-1374.
14. Hibino, H.; Inanobe, A.; Furutani, K.; Murakami, S.; Findlay, I.; Kurachi, Y., Inwardly Rectifying Potassium Channels: Their Structure, Function, and Physiological Roles. *Physiol. Rev.* **2010,** *90* (1), 291-366.
15. Bhave, G.; Lonergan, D.; Chauder, B. A.; Denton, J. S., Small-molecule modulators of inward rectifier K+channels: recent advances and future possibilities. *Future Medicinal*

Chemistry **2010,** *2* (5), 757-774.
16. Kobayashi, T.; Washiyama, K.; Ikeda, K., Inhibition of G protein-activated inwardly rectifying K+channels by fluoxetine (Prozac). *British Journal of Pharmacology* **2003,** *138* (6), 1119-1128.
17. Dobrev, D.; Carlsson, L.; Nattel, S., Novel molecular targets for atrial fibrillation therapy. *Nature Reviews Drug Discovery* **2012,** *11* (4), 275-291.
18. Chen, H.; Zuo, D.; Zhang, J.; Zhou, M.; Ma, L., Classification of 2-pore domain potassium channels based on rectification under quasi-physiological ionic conditions. *Channels* **2015,** *8* (6), 503-508.
19. Rajan, S.; Plant, L. D.; Rabin, M. L.; Butler, M. H.; Goldstein, S. A. N., Sumoylation Silences the Plasma Membrane Leak K+ Channel K2P1. *Cell* **2005,** *121* (1), 37-47.
20. Miller, A. N.; Long, S. B., Crystal structure of the human two-pore domain potassium channel K2P1. *Science* **2012,** *335* (6067), 432-6.
21. Bagriantsev, S. N.; Peyronnet, R.; Clark, K. A.; Honoré, E.; Minor, D. L., Multiple modalities converge on a common gate to control K2P channel function. *The EMBO Journal* **2011,** *30* (17), 3594-3606.
22. Brohawn, S. G.; del Marmol, J.; MacKinnon, R., Crystal Structure of the Human K2P TRAAK, a Lipid- and Mechano-Sensitive K+ Ion Channel. *Science* **2012,** *335* (6067), 436-441.
23. Feliciangeli, S.; Chatelain, F. C.; Bichet, D.; Lesage, F., The family of K2P channels: salient structural and functional properties. *The Journal of Physiology* **2015,** *593* (12), 2587-2603.
24. Braun, A. P., Two-pore domain potassium channels: variation on a structural theme. *Channels* **2012,** *6* (3), 139-140.
25. Piechotta, P. L.; Rapedius, M.; Stansfeld, P. J.; Bollepalli, M. K.; Erhlich, G.; Andres-Enguix, I.; Fritzenschaft, H.; Decher, N.; Sansom, M. S. P.; Tucker, S. J.; Baukrowitz, T., The pore structure and gating mechanism of K2P channels. *The EMBO Journal* **2011,** *30* (17), 3607-3619.
26. Nestler, E.; Mazella, J.; Pétrault, O.; Lucas, G.; Deval, E.; Béraud-Dufour, S.; Gandin, C.; El-Yacoubi, M.; Widmann, C.; Guyon, A.; Chevet, E.; Taouji, S.; Conductier, G.; Corinus, A.; Coppola, T.; Gobbi, G.; Nahon, J.-L.; Heurteaux, C.; Borsotto, M., Spadin, a Sortilin-Derived Peptide, Targeting Rodent TREK-1 Channels: A New Concept in the Antidepressant Drug Design. *PLoS Biology* **2010,** *8* (4), e1000355.
27. Sandoz, G.; Bell, S. C.; Isacoff, E. Y., Optical probing of a dynamic membrane interaction that regulates the TREK1 channel. *Proceedings of the National Academy of Sciences* **2011,** *108* (6), 2605-2610.
28. Rodrigues, N.; Bennis, K.; Vivier, D.; Pereira, V.; C. Chatelain, F.; Chapuy, E.; Deokar, H.; Busserolles, J.; Lesage, F.; Eschalier, A.; Ducki, S., Synthesis and structure–activity relationship study of substituted caffeate esters as antinociceptive agents modulating the TREK-1 channel. *European Journal of Medicinal Chemistry* **2014,** *75*, 391-402.
29. Åqvist, J.; Luzhkov, V., Ion permeation mechanism of the potassium channel. *Nature* **2000,** *404* (6780), 881-884.
30. Furini, S.; Domene, C., K+ and Na+ Conduction in Selective and Nonselective Ion Channels Via Molecular Dynamics Simulations. *Biophysical Journal* **2013,** *105* (8), 1737-1745.
31. Egwolf, B.; Roux, B., Ion Selectivity of the KcsA Channel: A Perspective from Multi-Ion Free Energy Landscapes. *Journal of Molecular Biology* **2010,** *401* (5), 831-842.
32. Jensen, M. O.; Borhani, D. W.; Lindorff-Larsen, K.; Maragakis, P.; Jogini, V.; Eastwood, M. P.; Dror, R. O.; Shaw, D. E., Principles of conduction and hydrophobic gating in K+ channels. *Proceedings of the National Academy of Sciences* **2010,** *107* (13), 5833-

5838.
33. Chanda, B.; Kwame Asamoah, O.; Blunck, R.; Roux, B.; Bezanilla, F., Gating charge displacement in voltage-gated ion channels involves limited transmembrane movement. *Nature* **2005,** *436* (7052), 852-856.
34. Treptow, W.; Tarek, M., Environment of the Gating Charges in the Kv1.2 Shaker Potassium Channel. *Biophysical Journal* **2006,** *90* (9), L64-L66.
35. Delemotte, L.; Tarek, M.; Klein, M. L.; Amaral, C.; Treptow, W., Intermediate states of the Kv1.2 voltage sensor from atomistic molecular dynamics simulations. *Proceedings of the National Academy of Sciences* **2011,** *108* (15), 6109-6114.
36. Fürst, O.; Nichols, Colin G.; Lamoureux, G.; D'Avanzo, N., Identification of a Cholesterol-Binding Pocket in Inward Rectifier K+ (Kir) Channels. *Biophysical Journal* **2014,** *107* (12), 2786-2796.
37. Dong, Y. Y.; Pike, A. C. W.; Mackenzie, A.; McClenaghan, C.; Aryal, P.; Dong, L.; Quigley, A.; Grieben, M.; Goubin, S.; Mukhopadhyay, S.; Ruda, G. F.; Clausen, M. V.; Cao, L.; Brennan, P. E.; Burgess-Brown, N. A.; Sansom, M. S. P.; Tucker, S. J.; Carpenter, E. P., K2P channel gating mechanisms revealed by structures of TREK-2 and a complex with Prozac. *Science* **2015,** *347* (6227), 1256-1259.
38. Chen, X.; Wang, Q.; Ni, F.; Ma, J., Structure of the full-length Shaker potassium channel Kv1.2 by normal-mode-based X-ray crystallographic refinement. *Proceedings of the National Academy of Sciences* **2010,** *107* (25), 11352-11357.
39. Whorton, Matthew R.; MacKinnon, R., Crystal Structure of the Mammalian GIRK2 K+ Channel and Gating Regulation by G Proteins, PIP2, and Sodium. *Cell* **2011,** *147* (1), 199-208.
40. Šali, A.; Blundell, T. L., Comparative protein modelling by satisfaction of spatial restraints. *Journal of molecular biology* **1993,** *234* (3), 779-815.
41. Whorton, M. R.; MacKinnon, R., X-ray structure of the mammalian GIRK2-[bgr][ggr] G-protein complex. *Nature* **2013,** *498* (7453), 190-197.
42. Fiser, A.; Sali, A., ModLoop: automated modeling of loops in protein structures. *Bioinformatics (Oxford, England)* **2003,** *19* (18), 2500-1.
43. Grubmüller, H., Solvate: a program to create atomic solvent models. *Electronic publication:* http://www.mpibpc.mpg.de/grubmueller/solvate **1996**.
44. Lupyan, D.; Mezei, M.; Logothetis, D. E.; Osman, R., A molecular dynamics investigation of lipid bilayer perturbation by PIP 2. *Biophysical journal* **2010,** *98* (2), 240-247.
45. Klauda, J. B.; Venable, R. M.; Freites, J. A.; Oâ™Connor, J. W.; Tobias, D. J.; Mondragon-Ramirez, C.; Vorobyov, I.; MacKerell, A. D.; Pastor, R. W., Update of the CHARMM All-Atom Additive Force Field for Lipids: Validation on Six Lipid Types. *The Journal of Physical Chemistry B* **2010,** *114* (23), 7830-7843.
46. Brooks, B.; Brooks, C.; MacKerell, A.; Nilsson, L.; Petrella, R.; Roux, B.; Won, Y.; Archontis, G.; Bartels, C.; Boresch, S., CHARMM: the biomolecular simulation program. *Journal of computational chemistry* **2009,** *30* (10), 1545-1614.
47. Jorgensen, W. L.; Chandrasekhar, J.; Madura, J. D.; Impey, R. W.; Klein, M. L., Comparison of simple potential functions for simulating liquid water. *The Journal of Chemical Physics* **1983,** *79* (2), 926-935.
48. Noskov, S. Y.; Berneche, S.; Roux, B., Control of ion selectivity in potassium channels by electrostatic and dynamic properties of carbonyl ligands. *Nature* **2004,** *431* (7010), 830-834.
49. Phillips, J. C.; Braun, R.; Wang, W.; Gumbart, J.; Tajkhorshid, E.; Villa, E.; Chipot, C.; Skeel, R. D.; Kalé, L.; Schulten, K., Scalable molecular dynamics with NAMD. *Journal of Computational Chemistry* **2005,** *26* (16), 1781-1802.

50. Darden, T.; York, D.; Pedersen, L., Particle mesh Ewald: An N·log(N) method for Ewald sums in large systems. *The Journal of Chemical Physics* **1993,** *98* (12).
51. Chovancova, E.; Pavelka, A.; Benes, P.; Strnad, O.; Brezovsky, J.; Kozlikova, B.; Gora, A.; Sustr, V.; Klvana, M.; Medek, P., CAVER 3.0: a tool for the analysis of transport pathways in dynamic protein structures. *PLoS Computational Biology* **2012,** *8* (10), e1002708.
52. Sievers, F.; Wilm, A.; Dineen, D.; Gibson, T. J.; Karplus, K.; Li, W.; Lopez, R.; McWilliam, H.; Remmert, M.; Soding, J.; Thompson, J. D.; Higgins, D. G., Fast, scalable generation of high-quality protein multiple sequence alignments using Clustal Omega. *Molecular Systems Biology* **2014,** *7* (1), 539-539.
53. Baker, N. A.; Sept, D.; Joseph, S.; Holst, M. J.; McCammon, J. A., Electrostatics of nanosystems: Application to microtubules and the ribosome. *Proceedings of the National Academy of Sciences* **2001,** *98* (18), 10037-10041.
54. Cheng, A. C.; Coleman, R. G.; Smyth, K. T.; Cao, Q.; Soulard, P.; Caffrey, D. R.; Salzberg, A. C.; Huang, E. S., Structure-based maximal affinity model predicts small-molecule druggability. *Nature Biotechnology* **2007,** *25* (1), 71-75.
55. Liang, J.; Woodward, C.; Edelsbrunner, H., Anatomy of protein pockets and cavities: Measurement of binding site geometry and implications for ligand design. *Protein Science* **1998,** *7* (9), 1884-1897.
56. Coleman, R. G.; Burr, M. A.; Souvaine, D. L.; Cheng, A. C., An intuitive approach to measuring protein surface curvature. *Proteins: Structure, Function, and Bioinformatics* **2005,** *61* (4), 1068-1074.
57. Kaczmarski, J. A.; Corry, B., Investigating the size and dynamics of voltage-gated sodium channel fenestrations. *Channels* **2014,** *8* (3), 264-277.
58. Barber, A. F.; Carnevale, V.; Raju, S. G.; Amaral, C.; Treptow, W.; Klein, M. L., Hinge-bending motions in the pore domain of a bacterial voltage-gated sodium channel. *Biochimica et Biophysica Acta (BBA) - Biomembranes* **2012,** *1818* (9), 2120-2125.
59. Corry, B.; Lee, S.; Ahern, C. A., Pharmacological insights and quirks of bacterial sodium channels. In *Voltage Gated Sodium Channels*, Springer: 2014; pp 251-267.
60. Yang, T.; Smith, J. A.; Leake, B. F.; Sanders, C. R.; Meiler, J.; Roden, D. M., An Allosteric Mechanism for Drug Block of the Human Cardiac Potassium Channel KCNQ1. *Molecular Pharmacology* **2013,** *83* (2), 481-489.
61. Lenaeus, M. J.; Burdette, D.; Wagner, T.; Focia, P. J.; Gross, A., Structures of KcsA in Complex with Symmetrical Quaternary Ammonium Compounds Reveal a Hydrophobic Binding Site. *Biochemistry* **2014,** *53* (32), 5365-5373.

TABLES

Table 1. Fenestration bottleneck features. Fenestration cluster ID (clustering threshold of 8 Å), percentage of PDB snapshots analyzed with a bottleneck radius (BR) > 0.8 Å, fenestration type (intra or inter-chain), average (Av.) bottleneck radius (Å), maximum (max.) bottleneck radius (Å) and length of the fenestration (Å) are reported. Protein monomers are referred as A, B, C, and D. Open and closed ion channel states are indicated by O and C.

Channel	Cluster ID	% snapshots BR > 0.8 Å	Fenestration Type	Av. BR (Å)	Max. BR (Å)	Length (Å)
Kv1.2	1	82	Lateral-A/D	1.0 ± 0.1	1.3	21 ± 4
	2	70	Lateral-B/C	1.0 ± 0.1	1.5	23 ± 4
	3	74	Lateral-A/C	1.0 ± 0.1	1.5	24 ± 3
	4	49	Lateral-B/D	0.9 ± 0.1	1.2	23 ± 4
	5	42	Lateral-A	1.3 ± 0.2	1.7	29 ± 6
Kir3.2/O	1	95	Lateral-B	1.0 ± 0.2	1.6	30 ± 3
	2	95	Lateral-D	1.0 ± 0.1	1.3	29 ± 3
	3	84	Lateral-A	1.0 ± 0.1	1.3	31 ± 3
	4	79	Lateral-C	1.0 ± 0.1	1.4	30 ± 3
	5	75	Lateral-C/D	0.9 ± 0.1	1.2	32 ± 3
Kir3.2/C	1	98	Lateral-D	1.0 ± 0.1	1.4	28 ± 2
	2	87	Lateral-C	1.0 ± 0.1	1.4	29 ± 3
	3	87	Lateral-B	0.9 ± 0.1	1.3	29 ± 3
	4	58	Lateral-A	0.9 ± 0.1	1.3	30 ± 3
	5	53	Lateral-B/C	0.9 ± 0.1	1.2	31 ± 5
TWIK-1	1	97	Lateral-A	1.2 ± 0.2	1.6	22 ± 2
	2	83	Lateral-B	0.9 ± 0.1	1.3	26 ± 2
	3	90	Lateral-A/B	1.4 ± 0.5	2.5	24 ± 2
	4	80	Lateral-A/B	1.0 ± 0.2	1.9	26 ± 4

Table 2. Pfido druggability analysis of fenestrations from MD snapshots of Kv1.2, Kir3.2, TWIK-1, compared to TREK-2 crystal structure. Individual Pfido components are: (a) Lipophilic Surface Area (SA; Å²) showing the total hydrophobic surface area of fenestration cavities, (b) Polar Surface Area (SA; Å²), (c) Total Surface Area (SA; Å²) which is the sum of hydrophobic and polar SAs, (d) Fraction of lipophilic SA, (e) Protein surface curvature, (f) Druggability score as a maximum affinity predicted (MAP) ΔG_{MAP} (kcal/mol), (g) Druggability score as a dissociation constant (K_d). The results indicate that the channels are characterised by high lipophilic surface area (except Kir3.2 which has charged polar fenestration residues), low fenestration curvature and high druggability score for fenestrations.

Protein	SA (lipo) Å²	SA (polar) Å²	SA (total) Å²	Fraction SA (lipo)	Curvature Å	Druggability ΔG_{MAP} (kcal/mol)	K_d (nM)
Kv1.2	399 ± 28	42 ± 6	441 ± 28	0.9 ± 0.0	6.2 ± 0.2	-15.8 ± 0.4	$2.5x10^{-3}$
Kir3.2	165 ± 21	122 ± 15	287 ± 15	0.6 ± 0.1	6.1 ± 0.2	-10.1 ± 0.9	38.4
TWIK-1	387 ± 25	30 ± 5	417 ± 29	0.9 ± 0.0	6.1 ± 0.1	-16.3 ± 0.1	$1.1x10^{-3}$
TREK-2	401	85	486	0.8	6.1	-14.5	$2.3x10^{-2}$

FIGURES

Figure 1. Structures of the ion channels involved in this study. (a) Kv1.2, (b) Kir3.2, (c) TWIK-1, and (d) TREK-2 channel structures. Illustrations of the fenestrations found in the transmembrane domains of structures obtained from MD trajectories (d, e, f) and those observed in the crystal structure of TREK-2 (h). Chain A, B, C and D are in red, yellow, orange, and black. Fenestration clusters 1, 2 and 3 are in yellow, cyan, and orange respectively. Fenestration cluster 4 is in the rear view of each channel.

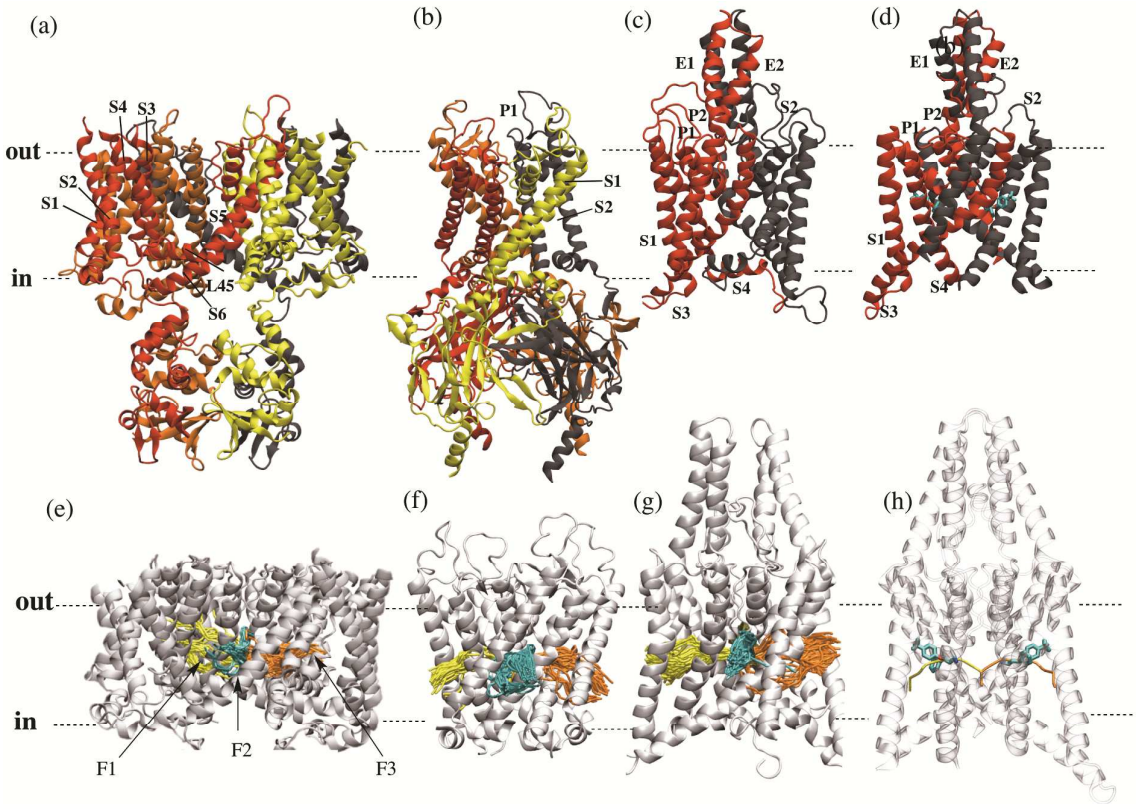

Figure 2. Lateral fenestrations and dynamics of the Bottleneck Radius (BR). Main lateral fenestrations oriented related to membrane plane, labelled and coloured by cluster ID, (a) Kv1.2 fenestrations 1 to 4, (b) Kir3.2/O fenestrations 1 to 5, and (c) TWIK-1 fenestrations 1 to 4. Temporal evolution of the BR for each fenestration cluster is presented as a colour-map with radii values ranging from 0.0 Å (red) to 3.0 Å (green), is shown for (d) Kv1.2, (e) Kir3.2/O, and (f) TWIK-1.

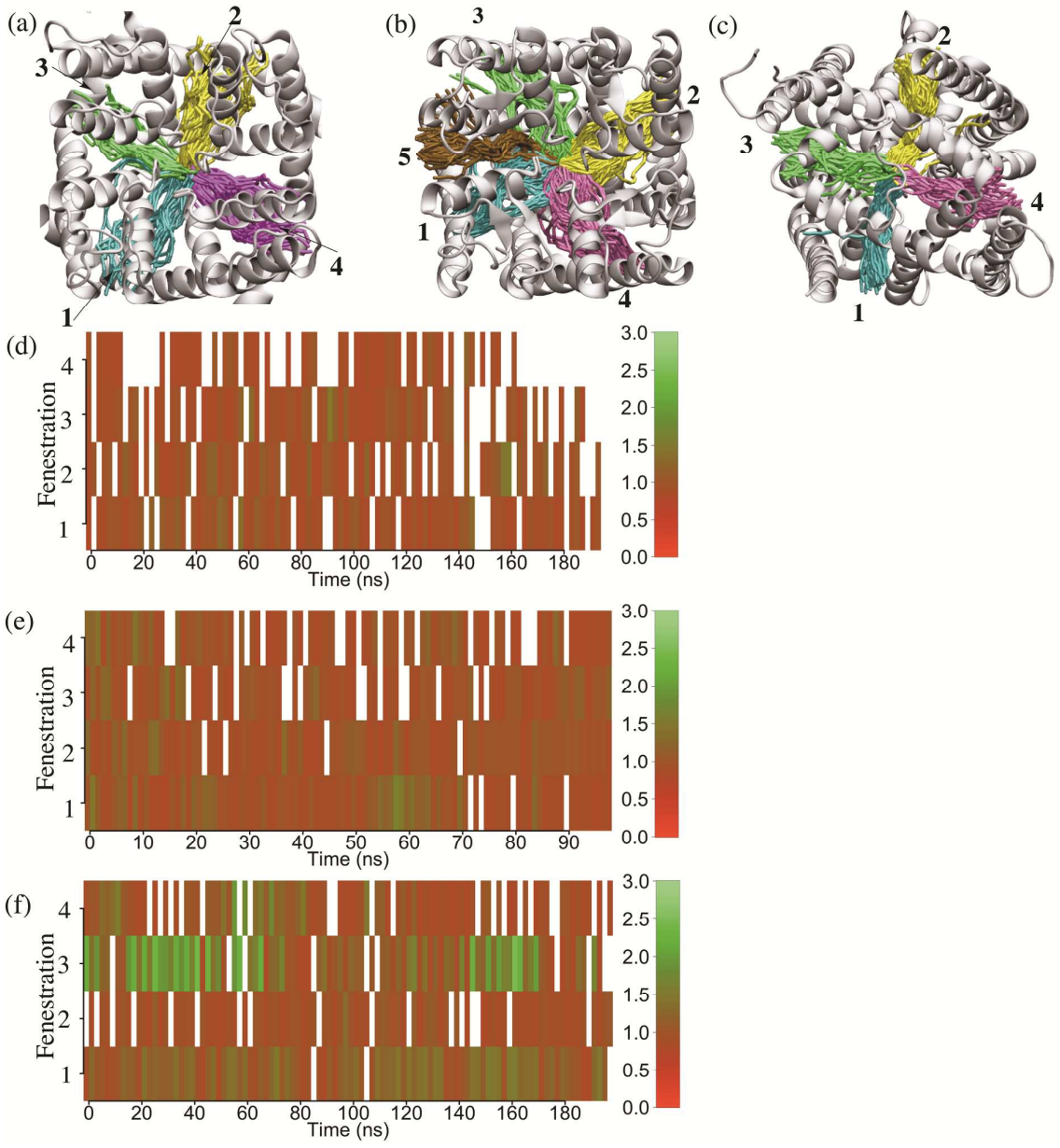

Figure 3. Sequence and structural alignment. (a) Multiple sequence alignment of the human Kv1.2 (Uniprot P16389), Kv1.3 (Uniprot P22001), Kv1.5 (Uniprot P22460), Kv7.1 (Uniprot P51787), mammalian Kir3.2 (Uniprot P48542), Kir3.1 (Uniprot P48549), Kir2.2 (Uniprot Q14500), human TWIK-1 (Uniprot O00180), TREK-2 (Uniprot P57789) and TWIK-2 (K2P6.1; Uniprot Q9Y257) highlighting the regions where the bottleneck lining residues are located. Color code: Kv1.2 (red), Kir3.2 (blue), TWIK-1 (green), TREK-2[37] (purple). Representative lining residues (>90% of each fenestration): (b) Kv1.2, (c) Kir3.2/O, and (d) TWIK-1 A/B lateral fenestration.

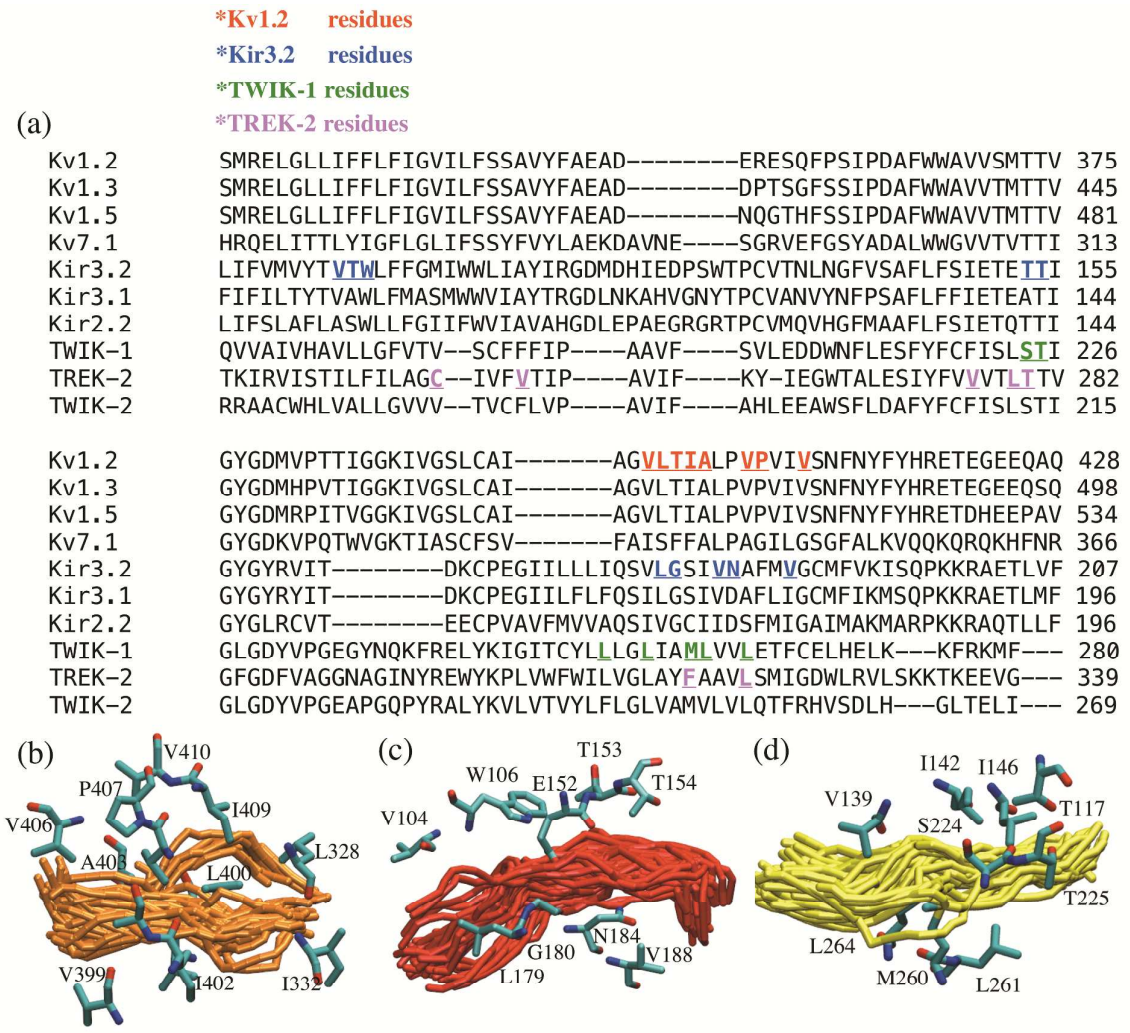

Figure 4. Fenestration dynamics as a function of time. (a, b, c) Radii spherical representation for fenestrations in Kv1.2, Kir3.2, and TWIK-1. Residues constituting the bottleneck are highlighted in licorice representation. (d,e,f) Evolution of fenestration bottleneck radii in Å, using a colour gradient ranging from 0 (blue) to 4 Å (red), during MD simulation of Kv1.2, Kir3.2/O, TWIK-1 respectively. The white gaps represent snapshots in which fenestrations with a probe radius > 0.8 Å threshold were not identified in the specific cluster.

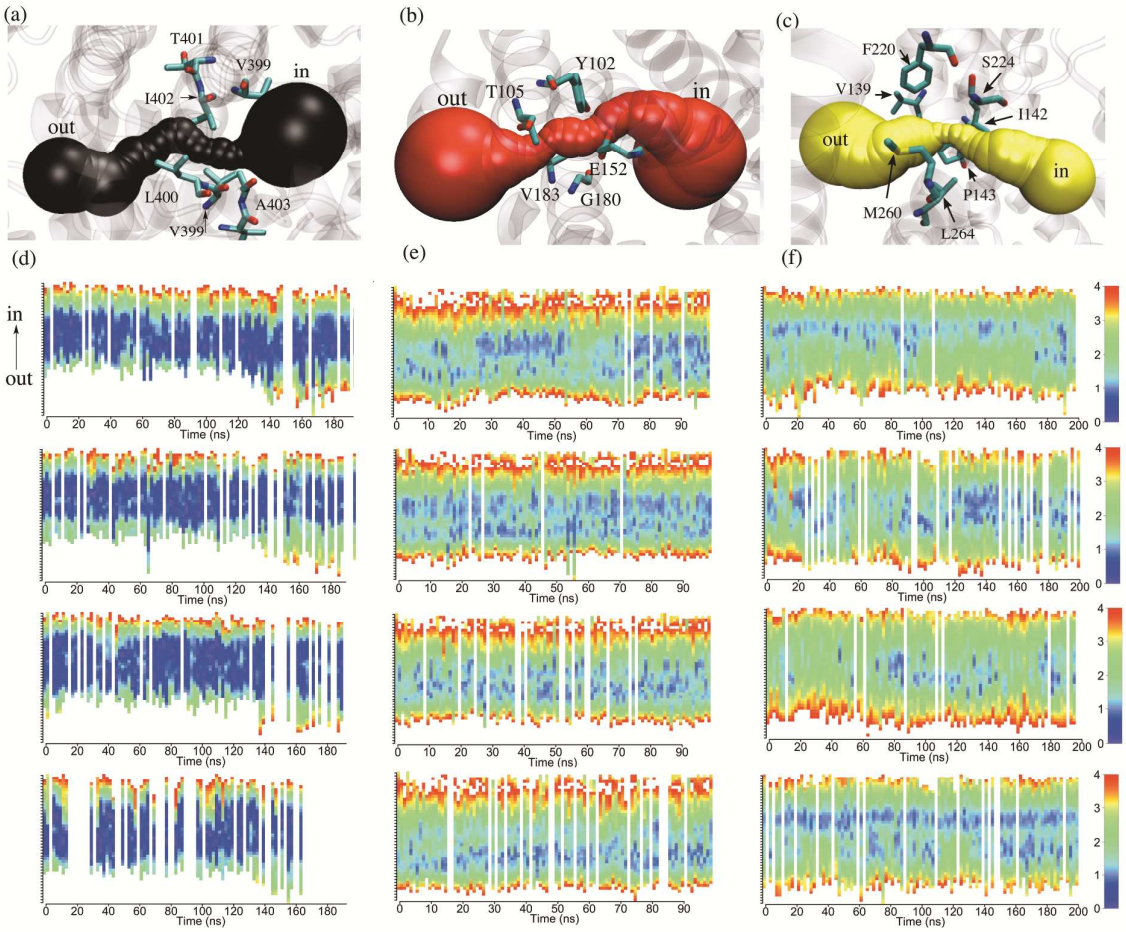

Figure 5. TWIK-1 fenestrations. Lipid-protein interaction iso-0.2 surfaces for fenestrations measured as the density of lipid within a 4 Å cutoff criteria of the fenestration-lining residues of TWIK-1 for (a) fenestrations 3,4 (inter-chain) and (b) fenestrations 1,2 (intra-subunit). (c) TWIK-1 lipid-protein interaction contacts to residues M260 and L264, (e) Distance between POPC tail (C atom) and C-atom of side-chain of M260 (colour red) as a function of simulation time in the TWIK-1 system. (f) Distance between the C atoms of side-chains of M260 and L264 in the A/B inter-chain lateral fenestrations 3 and 4 as a function of simulation time in the TWIK-1 system. Fenestration values for 3 vary from open (distance > 7 Å) to close (distance 4-5 Å). (g) Bottleneck radius for inter-chain fenestrations 3 (red) and 4 (blue) over the course of the trajectory. Changes in the bottleneck size are correlated with the side-chain motion of M260 and L264.